# Modeling and speciation of uranium (VI) and technetium (VII) co-extraction with DEHiBA

*P. Moeyaert[a], T. Dumas[a], D. Guillaumont[a], K. Kvashnina[b, c], C. Sorel[a], M. Miguirditchian[a], Ph. Moisy[a] and J.-F. Dufrêche[d]*

a French Alternative Energies and Atomic Energy Commission, CEA, Nuclear Energy Division, Radio Chemistry & Processes Department, DRCP, BP 17171, F-30207 Bagnols sur Cèze, France. E-mail: manuel.miguirditchian@cea.fr; Tel: +33 4 66 79 90 09

b European Synchrotron Radiation Facility, 38000 Grenoble, France

c Helmholtz Zentrum Dresden-Rossendorf, Institute of Resource Ecology, 01314 Dresden, Germany

d Institut de Chimie Séparative de Marcoule, Université de Montpellier 2, UMR 5257 CEA / CNRS / UM2 / ENSCM BP 17171 30207 Bagnols sur Cèze Cedex, France.

KEYWORDS - N, N-dialkylamides, DEHiBA, technetium, uranium, solvent extraction, modeling, speciation

## EXPERIMENTAL

### Reagents

DEHiBA was synthesized by Pharmasynthese (INABATA group) and diluted at 1 mol.$L^{-1}$ in TPH (Novasep process). Its purity (> 99%) was checked by Nuclear Magnetic Resonance (NMR) and mass spectrometry (GC-MS). An aqueous stock solution of pertechnetic acid was prepared starting with pure $NH_4^{99}TcO_4$ following the procedure described in [19, 20]. Solutions of $10^{-3}$ M $HTcO_4$ spiked with $^{99m}Tc$ (provided by Cis-Bio IBA) were prepared at different nitric acid concentrations from 0.01 to 8 M for technetium solvent extraction experiments. Uranium stock solution used to prepare solutions with nitric acid and technetium was prepared from uranyl nitrate purchased from Prolabo and titrated using X-Ray fluorescence (Quant'X from ThermoFisher Scientific). All other high grade chemical reagents ($HNO_3$, NaOH, EtOH, …) were purchased from Prolabo and used without further purification.

### Methods

#### *Solvent extraction experiments*

Solvent extraction experiments were performed by vigorous shaking of equal volumes of organic and aqueous phases containing metal ions for one hour at $T$=298.15 K, $T$ being controlled by a water bath. After centrifugation, the two phases were separated and aliquots of each phase were sampled for analysis. Nitric acid concentrations in aqueous and organic phases were measured by acid-base titration against 0.1 M NaOH solution, by diluting the aliquot in water and water/ethanol mixture (50/50%$_{vol}$) respectively or in saturated ammonium oxalate in presence of uranium. Uranium concentration in both phases was determined by UV-vis spectrophotometry (CARY 500 from AGILENT) while $^{99m}Tc$ activities were measured by

gamma spectrometry (Hyper pure Ge detector, CANBERRA). The distribution ratio of technetium ($D_{Tc}$) is defined according to equation (1):

$$D_{Tc} = \overline{A_{Tc}}/A_{Tc} \quad (1)$$

where $\overline{A}$ and A are the γ radioactivities of $^{99m}$Tc, in the organic and aqueous phase respectively (expressed in terms of decays per volume unit per second). It is assumed from previous experiments that D-values between 0.1 and 10 exhibit a maximum error of about 5% while the error may be up to 10% for lower (0.01-0.1) and higher (10-100) values.

*Infrared spectroscopy*

**Table 1** summarizes the compositions of the different samples used for EXAFS and IR experiments. Infrared measurements were performed on the organic samples 1, 2 and 3' using a Bruker Equinox 55 FT-IR spectrometer equipped with an attenuated total reflectance cell. The samples were prepared by solvent extraction following the procedure described above. All spectra were collected between 650 and 4000 $cm^{-1}$ using 32 scans and a resolution of 2 $cm^{-1}$.

*XAS data acquisition*

EXAFS spectra for organic samples 1, 2, 3 and 4 (see **Table 1** for experimental conditions) were recorded at the European Synchrotron Radiation Facility (ESRF, Grenoble, France) (6 GeV at 200 mA), at the Rossendorf beamline (BM20). BM20 is equipped with a water-cooled Si(111) double crystal monochromator (DCM). Beam collimation and rejection of higher-order harmonics were achieved with two Pt-coated cylindrical-shaped mirrors before and after the DCM. A 13-element Ge solid state detector (CANBERRA) was used for data collection in fluorescence mode.

Monochromator energy calibration was carried out using an yttrium metallic foil for uranium $L_3$ edge (Y K edge at 17038 eV) and a molybdenum foil for technetium K edge (Mo K edge at 20000 eV).

All measurements were performed at room temperature in 200 µL double layered cells specifically designed for radioactive samples. [21] The data represent averages of 4 scans at uranium $L_3$ edge and 3 to 5 scans for technetium K edge.

**Table 1.** Summary of the compositions of EXAFS and FT-IR samples.

| Sample | $[\overline{DEHiBA}]$ mol.L$^{-1}$ | $[\overline{HNO_3}]$ mol.L$^{-1}$ | $[\overline{U}]$ mol.L$^{-1}$ | $[\overline{Tc}]$ mol.L$^{-1}$ |
|---|---|---|---|---|
| 1 | 1 | $9.62\ 10^{-2}$ | $3.65\ 10^{-2}$ | 0 |
| 2 | 1 | $8.57\ 10^{-2}$ | $4.24\ 10^{-2}$ | $2.60\ 10^{-2}$ |
| 3 | 1 | $6.27\ 10^{-2}$ | $1.69\ 10^{-2}$ | $4.07\ 10^{-2}$ |
| 3’ | 1 | $8.57\ 10^{-2}$ | $4.24\ 10^{-2}$ | $5.20\ 10^{-2}$ |
| 4 | 1 | $7.81\ 10^{-2}$ | 0 | $4.20\ 10^{-3}$ |

XAS data treatment

XAS data processing was carried out with the Athena code. [29] After energy calibration, the $E_0$ energy was set at the maximum of the absorption edge for uranium: 17177.9 eV, and at 21070 eV for technetium (to minimize $\Delta E_0$ in the fitting procedure). The EXAFS signal was extracted by subtracting a linear pre-edge background and a combination of cubic spline functions for atomic absorption background and then normalized by the Lengeler-Eisenberg procedure. Pseudo-radial distribution functions (PRDF) were obtained by Fourier transform in $k^3\chi(k)$ using the ATHENA code [29] between 2 and 13 Å$^{-1}$ for technetium samples and between 2.5 and 17 Å$^{-1}$

for uranium ones. The R factor (%) and the quality factor (QF, reduced chi$^2$) of the fits are provided from ARTEMIS. [29]

Back-scattering amplitude and phase shift function were obtained from FEFF 8.2 calculation [30] performed on two model structures. The $\overline{L_2(UO_2)(NO_3)_2}$ model is taken from single crystal XRD [21] and the $\overline{L_2(UO_2)(NO_3)(TcO_4)}$ model from the optimized DFT structures (see DFT section). At uranium $L_3$ edge, all fitting operations are performed in R-space over individual radial distances for each ligand ($\Delta R_{Oyl}$, $\Delta R_{DEHiBA}$, $\Delta R_{NO3}$, $\Delta R_{TcO4}$) and Debye-Waller factors ($\sigma^2_{Oyl}$, $\sigma^2_{DEHiBA}$, $\sigma^2_{NO3}$, $\sigma^2_{TcO4}$). To take into account the distribution data model $NO_3$ and $TcO_4$, coordination numbers were also adjusted. Coordination number for oxygen atoms from uranyl and DEHiBA and amplitude reduction factor ($S_0^2$) were fixed (2, 2 and 1 respectively). For technetium K edge, only the $\overline{L_2(UO_2)(NO_3)(TcO_4)}$ model from the optimized DFT structures was used. Only the first coordination shell was considered in the fitting procedure with four oxygen atoms ($\Delta R_O$ and $\sigma^2_O$). Coordination number and amplitude reduction factor were fixed to 4 and one respectively.

## RESULTS

### *Infrared spectroscopy*

The infrared spectra of DEHiBA-uranyl nitrato-pertechnetate complexes were compared with those of DEHiBA-uranyl nitrato complexes. In **Table 2** are summarized the principal vibrational frequencies of the DEHiBA-uranyl nitrato complexes. [33] From infrared spectroscopy, information can be obtained about carbonyl, nitrate and uranyl stretching vibrations. As shown in **Figure 1**, asymmetric stretching frequency of $UO_2^{2+}$ ion occurs at 935 cm$^{-1}$ in the DEHiBA-uranyl nitrato complex. When uranium and technetium are co-extracted, no significant change is

observed but a slight shift of the carbonyl C=O stretch (from 1572 to 1564 $cm^{-1}$) is noticed when the Tc/U ratio increases.

**Table 2.** Selected vibrational frequencies of the DEHiBA-uranyl nitrato complexes

| Type of vibration | ν / $cm^{-1}$ |
|---|---|
| ν free C=O | 1650 |
| ν bonded C=O | 1573 |
| $\nu_1$ N=O | 1525 |
| $\nu_4$ N-O | 1272 |
| $\nu_2$ N-O | 1029 |
| $\nu_{as}$ $UO_2^{2+}$ | 935 |
| ν N-O | 745 |

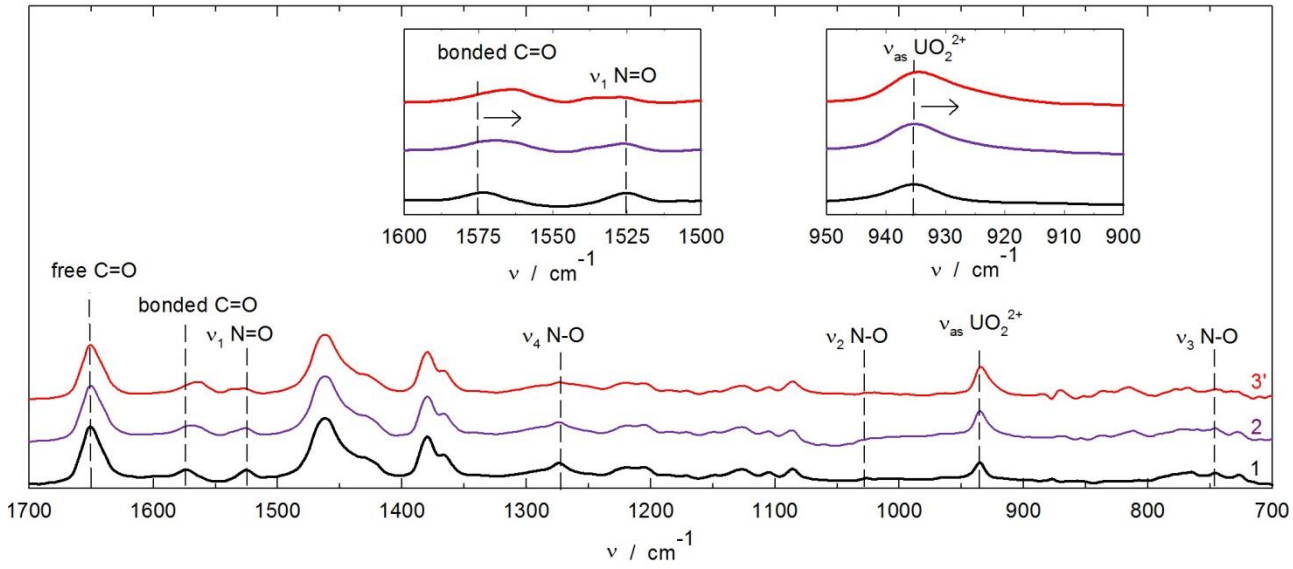


**Figure 1.** Infrared spectra for samples 1 (DEHiBA-uranyl nitrato complexes, $[\overline{Tc}]/[\overline{U}]=0$), 2 and 3' (DEHiBA-uranyl pertechnetate nitrato complexes, $[\overline{Tc}]/[\overline{U}]=0.6$ and 1.2 respectively). See Table 1 for the sample compositions.

Varying the Tc/U ratio also induces some changes in the intensity and in the shape of the nitrate $\nu_1$ N=O stretch. The changes observed, although very weak, suggest that modifications in the immediate uranyl coordination environment occur with the increase of Tc concentration in organic phase.

*DFT calculations*

DFT calculations were undertaken in order to further investigate the coordination geometry in the inner uranium coordination sphere.

Geometries of $\overline{(\mathrm{DEHiBA})_2(\mathrm{UO_2})(\mathrm{NO_3})(\mathrm{TcO_4})}$ were optimized and compared to $\overline{(\mathrm{DEHiBA})_2(\mathrm{UO_2})(\mathrm{NO_3})_2}$. In a previous study, it was shown that in the absence of Tc, uranyl is surrounded by two DEHiBA and two bidentate nitrate ions. [21, 34] Initial structures were constructed where $TcO_4^-$ replaces one nitrate ion in a bidentate coordination mode. However, in the course of the geometry optimization, $TcO_4^-$ which is bulkier than $NO_3^-$ becomes monodentate. The resulting optimized geometry and structural parameters are shown on **Figure 2** and **Table 3** for both complexes.

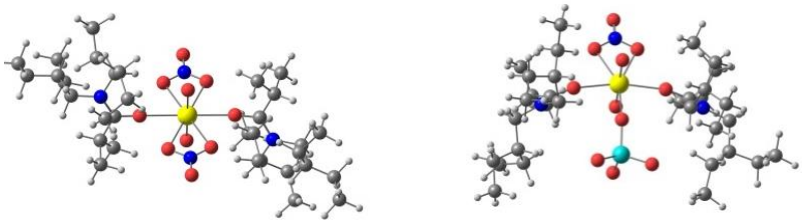

**Figure 2.** Optimized structures of $\overline{(\mathrm{DEHiBA})_2(\mathrm{UO_2})(\mathrm{NO_3})_2}$ (left) and $\overline{(\mathrm{DEHiBA})_2(\mathrm{UO_2})(\mathrm{NO_3})(\mathrm{TcO_4})}$ (right) complexes

**Table 3.** Calculated selected distances (average values in Å) and vibrational frequencies (in $cm^{-1}$) in $\overline{(\mathrm{DEHiBA})_2(\mathrm{UO_2})(\mathrm{NO_3})_2}$ and $\overline{(\mathrm{DEHiBA})_2(\mathrm{UO_2})(\mathrm{NO_3})(\mathrm{TcO_4})}$ from DFT/B3LYP in heptane (vibrational frequencies calculated in water solvent model in parentheses)

| | $\overline{(DEHiBA)_2(UO_2)(NO_3)_2}$ | $\overline{(DEHiBA)_2(UO_2)(NO_3)(TcO_4)}$ |
|---|---|---|
| U=O | 1.77 | 1.77 |
| U-O(DEHiBA) | 2.40 | 2.36 |
| U-O($NO_3$) | 2.54 | 2.52 |
| U-O($TcO_4$)) | - | 2.33 |
| U-Tc | - | 3.99 |
| ν bonded C=O | 1606 (1587) | 1589 (1576) |
| $\nu_{as}$ $UO_2^{2+}$ | 947 (933) | 947 (930) |

Vibrational frequencies were computed for the two species. Values for C=O stretching and uranyl asymmetric stretching frequencies are given in **Table 3**. Calculations were performed in the presence of a continuum solvent model corresponding to heptane and to water. The dielectric constant of the organic solution is not known, but should be in between heptane and water. As shown in **Table 3**, vibrational frequencies are strongly influenced by the dielectric constant of the solvent model. However, similar trends are obtained in both media, carbonyl stretching frequency is redshifted by 11 to 17 $cm^{-1}$ while uranyl stretching frequency is not significantly shifted in the presence of a monodentate $TcO_4^-$. These variations are consistent with experimental spectra and with the presence of $TcO_4^-$ in the coordination sphere of uranium. Calculated distances are not significantly altered by the solvent model and only values in heptane are reproduced. Uranium-Oxygen distances in the equatorial plane are slightly shortened by 0.02 to 0.04 Å in the presence of $TcO_4^-$. This is due to the monodentate coordination mode of $TcO_4^-$ which decreases uranyl coordination number from 6 to 5.

*EXAFS data analysis*

Technetium and uranium absorption edge shape and the edge position (chemical shift) can be used to confirm (i) local structure of the absorbing atoms and (ii) the oxidation state of the absorbing atoms.

The technetium edges were identical for all the samples and very similar to the published data for pertechnetate species. [35] The intense pre-edge observed at 21050 eV is due to 1s → nd transition only observed in tetrahedral geometry. Moreover the maximum edge energy at 21090 eV is consistent to previous results for $TcO_4$ compounds in solid state or aqueous phases. [35, 36]

For uranium, the maximum intensity of the absorption edge at 17177 eV is consistent with U(VI). After the intense white line, two other features at (17192 eV and 17210 eV) are observed respectively due to resonant scattering along the linear transdioxo unit ($UO_2^{2+}$) and to atoms in the equatorial plan. [37]

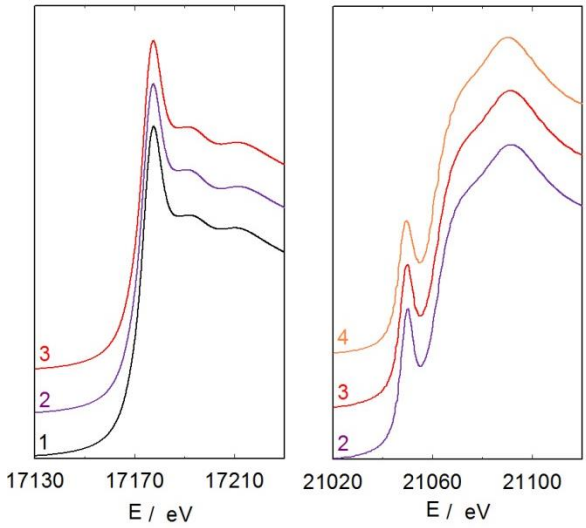


**Figure 3.** Technetium K and uranium $L_3$ absorption edges for sample 1, 2, 3 and 4.

Besides the edge itself, the extended fine structures (EXAFS) were used to determine technetium and uranium first and second coordination shell.

For technetium K edge, EXAFS spectra $\chi(k)\cdot k^3$ and corresponding Fourier transforms (with fits) are presented in ESI, and the fit results are listed in **Table 4**. Both coordination number of oxygen atoms (4) and Tc=O distance (1.73 Å) are consistent with the pertechnetate geometry. [36] Nevertheless, the Tc-U distance at 3.60 Å proposed by Suzuki and al [18] in co-extracted U/Tc complexes in TBP media is not observed.

The $k^3$-weighted Fourier transforms of EXAFS spectra obtained for samples 1, 2 and 3 for uranium $L_3$ edges are depicted in **Figure 4** (EXAFS spectra $\chi(k)\cdot k^3$ are given in ESI).

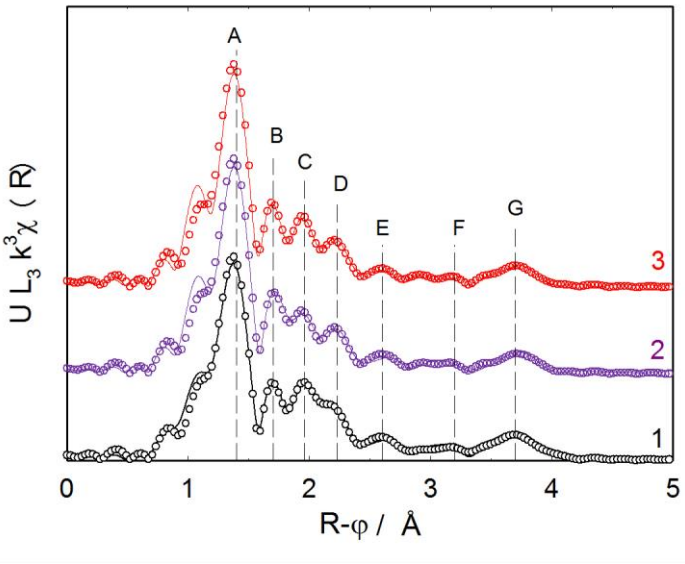


**Figure 4.** Experimental (—) and fitted (◦◦◦) Fourier transform of the $k^3$-weighted EXAFS spectra at uranium $L_3$ edge for organic samples 1 (DEHiBA-uranyl nitrato complexes, $[\overline{Tc}]/[\overline{U}]=0$), 2 and 3 (DEHiBA-uranyl pertechnetate nitrato complexes, $[\overline{Tc}]/[\overline{U}]=0.6$ and 2.4 respectively).

EXAFS oscillations are dominated by the trans-dioxo uranyl bond in the four samples corresponding on the FT to an intense peak (A) at R+φ = 1.4 Å. Atoms in uranyl equatorial plane result in 3 distinct peaks (B, C and D) observed between R+φ = 1.6 Å and R+φ = 2.5 Å on the Fourier transform. The Tc loading of the samples affects the intensity of peak C suggesting a modification in the uranium first coordination sphere. The second and third coordination shell

observed at R+φ > 2.5 Å (peaks E, F and G) are likely to be related to uranyl MS effect, DEHiBA C back scattering and bidentate nitrate oxygen atoms.

The spectra were fitted according to the procedure described in the calculation section. The theoretical spectra are displayed on **Figure 4** and the fit results are summarized in **Table 4**.

The $\overline{L_2(UO_2)(NO_3)_2}$ model taken from single crystal XRD [21] and the $\overline{L_2(UO_2)(NO_3)(TcO_4)}$ model including pertechnetate bounded to uranium in monodentate fashion were used. To determine the coordination sphere in the four samples, both distances and Debye Waller factor were adjusted for each scattering paths. Coordination number for the monoamide and yl oxygen were fixed while the nitrate and pertechnetate coordination number are interconnected floating parameters ($N_{NO3} = 2 - N_{TcO4}$). For the four samples, this model fits very well the experimental data with R-factor ≤ 2%. Distances obtained after data refinement are in agreement with XRD references and DFT models within error bars. The two axial "yl" oxygen atoms are stable at 1.77 Å while slight changes are observed in the equatorial oxygen shell as shown by direct reading of experimental data. By raising the Tc loading in the sample, the bidentate nitrate coordination number decreases with a concomitant increase of the monodentate pertechnetate oxygen atom. The result is a decrease of the total coordination number for uranyl equatorial oxygen (6 in sample 1 to 5.7 and 5.3 for the sample 2 and 3 respectively). As a result, the mean uranyl equatorial oxygen distance decreases from 2.48 Å for sample 1 to 2.45 Å for the most Tc loaded sample.

According to Suzuki and al. [18] EXAFS study in TBP, both pertechnetate and nitrate groups coordinate the uranyl cation in a bidentate fashion. In TBP, the first uranyl coordination shell is maintained (CN=6 and R-$O_{ax}$ = 2.48 Å) which contrast with the studied monoamide system. Moreover, the Tc backscattering effect expected at 3.60 Å for bidentate pertechnetate is never

observed. In the proposed monodentate model, the Tc is expected at about 4.1 Å (overlapping with the second nitrate oxygen ($O'_{NO3}$) shell oxygen at 4.2 Å –peak G).

**Table 4.** EXAFS fit parameters for samples 1 to 4. (*) indicates fixed parameters. (#) indicates interrelated parameters ($N_{U\text{-}O_{NO3}} = 2 \times (2 - N_{TcO4})$, $N_{U\text{-}N_{NO3}} = 2 - N_{TcO4}$, $N_{U\text{-}O'_{NO3}} = 2 - N_{TcO4}$, $N_{U\text{-}O_{TcO4}} = N_{TcO4}$ and $N_{U\text{-}Tc} = N_{TcO4}$). Fitting range: 2.5 $Å^{-1}$ to 16.5 $Å^{-1}$ at the U $L_3$ edge 2 $Å^{-1}$ to 11 $Å^{-1}$ at the Tc K edge.

| **Technetium** | **1** | | | **2** | | | **3** | | | **4** | | |
|---|---|---|---|---|---|---|---|---|---|---|---|---|
| **Tc K edge** | - | | | $S_0^2 = 1$; $\Delta E^0 = 0.6$ eV; $R_f = 2\%$ | | | $S_0^2 = 1$; $\Delta E^0 = -0.5$ eV; $R_f = 3\%$ | | | $S_0^2 = 1$ ; $\Delta E^0 = 2.4$ eV; $R_f = 2\%$ | | |
| **Path** | - | - | - | N | $\sigma^2$ (Å²) | R (Å) | N | $\sigma^2$ (Å²) | R (Å) | N | $\sigma^2$ (Å²) | R (Å) |
| ***Tc-O*** | - | - | - | *4.5* | *0.002** | 1.76 (2) | *4.5* | *0.002** | 1.76 (2) | *5.1* | *0.002** | 1.77 (2) |

| **Uranium** | **1** | | | **2** | | | **3** | | | **4** | | |
|---|---|---|---|---|---|---|---|---|---|---|---|---|
| **U $L_3$ edge** | $S_0^2 = 1$ ; $\Delta E^0 = 4.2$ eV; $R_f = 1\%$ | | | $S_0^2 = 1$; $\Delta E^0 = 4.49$ eV; $R_f = 1\%$ | | | $S_0^2 = 1$; $\Delta E^0 = 4.16$ eV; $R_f = 2\%$ | | | - | | |
| **Path** | N | $\sigma^2$ (Å²) | R (Å) | N | $\sigma^2$ (Å²) | R (Å) | N | $\sigma^2$ (Å²) | R (Å) | - | - | - |
| ***U=O*** | *2** | *0.002* | 1.77 (1) | *2** | *0.001* | 1.77 (1) | *2** | *0.002* | 1.77 (1) | - | - | - |
| ***U-O$_{mono}$*** | *2** | *0.007* | 2.39 (4) | *2** | *0.005* | 2.38 (1) | *2** | *0.004* | 2.35 (1) | - | - | - |
| ***U-O$_{NO3}$*** | *4#* | *0.007* | 2.52 (2) | *3.4#* | *0.006* | 2.53 (1) | *2.7#* | *0.006* | 2.51 (2) | - | - | - |
| ***U-O$_{TcO4}$*** | *0#* | - | - | *0.3#* | *0.009* | 2.51 (3) | *0.6#* | *0.006* | 2.48 (2) | - | - | - |
| ***U-N$_{NO3}$*** | *2#* | *0.005* | 2.97 (2) | *1.7#* | *0.006* | 2.95 (3) | *1.4#* | *0.004* | 2.96 (4) | - | - | - |
| ***U-C$_{mono}$*** | *2** | *0.007* | 3.99 (10) | *2** | *0.006* | 3.97 (10) | *2** | *0.010* | 4.00 (10) | - | - | - |
| ***U-O'$_{NO3}$*** | *2#* | *0.008* | 4.20 (10) | *1.7#* | *0.010* | 4.20 (7) | *1.4#* | *0.010* | 4.20 (6) | - | - | - |
| ***U-Tc*** | *0#* | - | - | *0.3#* | *0.009* | 4.12 (3) | *0.6#* | *0.006* | 4.08 (2) | - | - | - |

## CONCLUSIONS

A full comprehensive study was performed on the extraction of technetium (VII) by the N,N-dialkylamide DEHiBA in organic phase.

Experimental extraction isotherms were first acquired in batch conditions to evaluate the influence of nitric acid and uranium concentration on technetium distribution ratio. The increase in technetium extraction with the addition of uranium in organic phase and the decrease of nitric acid concentration in aqueous phase was correctly modeled using a thermodynamic approach based on the mass action law and using the simple solution concept to correct the deviations from ideal solutions in aqueous phase. Without uranium, the presence of three complexes was assumed in organic phase $\overline{(\mathrm{DEHiBA})_4(\mathrm{HTcO_4})}$, $\overline{(\mathrm{DEHiBA})_3(\mathrm{HTcO_4})(\mathrm{HNO_3})}$ and $\overline{(\mathrm{DEHiBA})_2(\mathrm{HTcO_4})(\mathrm{HNO_3})}$ while extraction of technetium (VII) with uranium (VI) was represented by taking into account the two complexes $\overline{(\mathrm{DEHiBA})_2(\mathrm{UO_2})(\mathrm{NO_3})(\mathrm{TcO_4})}$ and $\overline{(\mathrm{DEHiBA})_3(\mathrm{UO_2})(\mathrm{NO_3})(\mathrm{TcO_4})(\mathrm{HNO_3})}$.

To complete the classical thermodynamic description of a metal extraction by a neutral extractant and to probe the formation of the $\overline{(\mathrm{DEHiBA})_2(\mathrm{UO_2})(\mathrm{NO_3})(\mathrm{TcO_4})}$ species, the molecular structures were further investigated through spectroscopic measurements and theoretical calculations. FT-IR experiments showed that the uranyl inner sphere was affected by the presence of technetium. DFT calculations predicted that one $TcO_4^-$ anion replaces one nitrate ion in a monodentate coordination mode in the $\overline{(\mathrm{DEHiBA})_2(\mathrm{UO_2})(\mathrm{NO_3})_2}$ complex. EXAFS analysis, supported by theoretical calculations, confirmed the formation of this complex, and also the inner-sphere coordination mode: a pertechnetate group coordinates the uranyl cation in a monodentate fashion. A previous structural study suggests that during the co-extraction of uranium and technetium by TBP, both pertechnetate and nitrate groups coordinate the uranyl cation in a bidentate fashion. With the monoamide DEHiBA, the pertechnetate group should preferentially coordinate the uranyl cation in a monodentate fashion. Such a monodentate

coordination mode should be favored by steric effects induced by the presence of amides with large alkyl groups and of $TcO_4^-$ which is bulkier than $NO_3^-$.

Combining a macroscopic study (distribution data acquisition and modeling) with molecular-scale investigations (FT-IR and X-ray absorption analysis supported by theoretical calculations) has provided a new insight into the description of solvent extraction mechanism. This study shows the interest of investigating the speciation both at a macroscopic and at a molecular scale. This set of complementary methods could also be applied to other extractant systems, especially to observe the influence of the amide structure (branched or linear alkyl chains) on the coordination mode. It will allow to better simulate the behavior of technetium in the solvent extraction process in order to further master its separation and decontamination in the future reprocessing plants.

ACKNOWLEDGEMENTS

The authors are grateful to L. Chareyre and J. Chapelet for their support for $^{99m}Tc$ experiments and to C. Lefèbvre for support during the EXAFS experiment. The authors express their thanks to Dr. F. Poineau for his explanations and fruitful discussions on the work related to XAS data analysis. Many thanks go to Dr. C. Tamain for her valuable assistance in FT-IR analysis. The authors acknowledge Areva NC and the European Talisman project for financial support.

REFERENCES

1. K. H. Lieser, A. Krüger and R. N. Singh, *Radiochimica Acta*, 1981, **28**, 97-101.
2. J. G. Darab and P. A. Smith, *Chemistry of Materials*, 1996, **8**, 1004-1021.
3. K. Schwochau, *Technetium: Chemistry and Radiopharmaceutical Applications*, 2000.
4. CEA, *Treatment and recycling of spent nuclear fuel. Actinide partitioning – Application to waste management*, Le moniteur, Gif-sur-Yvette, 2008.
5. T. N. Jassim, G. Persson and J. O. Liljenzin, *Solv. Extr. Ion Exch.*, 1984, **2**, 1079-1092.
6. D. J. Pruett, *Radiochimica Acta*, 1981, **28**, 153-157.
7. T. H. Siddall, *The Journal of Physical Chemistry*, 1960, **64**, 1863-1866.
8. D. J. Pruett, *The solvent extraction of heptavalent technetium and rhenium by tributyl phosphate* ORNL/TM-8668, Tenessee, 1984.

9. N. Condamines and C. Musikas, *Solvent extraction and ion exchange*, 1988, **6**, 1007-1034.
10. N. Condamines and C. Musikas, *Solvent extraction and ion exchange*, 1992, **10**, 69-100.
11. P. N. Pathak, D. R. Prabhu, P. B. Ruikar and V. K. Manchanda, *Solvent extraction and ion exchange*, 2002, **20**, 293-311.
12. T. H. Siddall and M. O. N. Fulda, G. S., *Nuclear technology - Chemistry and chemical engineering*, 1961.
13. M. Miguirditchian, C. Sorel, I. Bisel, B. Cames, P. Baron, D. Espinoux, J.-C. Calor, C. Viallesoubranne, C. Lorrain and M. Masson, *Global'09*, 2009.
14. M. Montuir, C. Sorel, V. Pacary, X. Hérès, H. Roussel, B. Dinh and P. Baron, *ISEC'11*, 2011.
15. B. Mokili and C. Poitrenaud, *Solvent extraction and ion exchange*, 1995, **13**, 731-754.
16. B. Mokili and C. Poitrenaud, *Solvent extraction and ion exchange*, 1996, **14**, 617-634.
17. F. Macasek and J. Kadrabova, *Journal of Radioanalytical Chemistry*, 1979, **51**, 97-106.
18. S. Suzuki, T. Yaita, Y. Okamoto, H. Shiwaku and H. Motohashi, *Physica Scripta*, 2005, **T115**, 306-307.
19. G. E. Boyd, *Inorganic Chemistry*, 1978, **17**, 1808-1810.
20. P. Moeyaert, L. Abiad, C. Sorel, J. F. Dufrêche, A. Ruas, P. Moisy and M. Miguirditchian, *The Journal of Chemical Thermodynamics*, 2015, **91**, 94-100.
21. E. Acher, Y. Hacene Cherkaski, T. Dumas, C. Tamain, D. Guillaumont, N. Boubals, H. C., P. L. Solari and M. C. Charbonnel, *Inorganic Chemistry*, Submitted.
22. A. Ruas, O. Bernard, B. Caniffi, J. P. Simonin, P. Turq, L. Blum and P. Moisy, *Journal of Physical Chemistry B*, 2006, **110**, 3435-3443.
23. N. Charrin, P. Moisy, S. Garcia-Argote and P. Blanc, *Radiochimica Acta*, 1999, **86**, 143-149.
24. N. Kumari, P. N. Pathak, D. R. Prabhu and V. K. Manchanda, *Separation Science and Technology*, 2011, **46**, 79-86.
25. M. J. Frisch, G. W. Trucks, H. B. Schlegel, G. E. Scuseria, M. A. Robb, J. R. Cheeseman, G. Scalmani, V. M. Barone, B., G. A. Petersson, H. Nakatsuji, M. L. Caricato, X., H. P. Hratchian, A. F. Izmaylov, J. Bloino, G. Zheng, J. L. Sonnenberg, M. Hada, M. Ehara, K. Toyota, R. Fukuda, J. Hasegawa, M. Ishida, T. Nakajima, Y. Honda, O. Kitao, H. Nakai, T. Vreven, J. A. Montgomery, Jr., J. E. Peralta, F. Ogliaro, M. Bearpark, J. J. Heyd, E. Brothers, K. N. Kudin, V. N. Staroverov, R. Kobayashi, J. Normand, K. Raghavachari, A. Rendell, J. C. Burant, S. S. Iyengar, J. Tomasi, M. Cossi, N. Rega, J. M. Millam, M. Klene, J. E. Knox, J. B. Cross, V. Bakken, C. Adamo, J. Jaramillo, R. Gomperts, R. E. Stratmann, O. Yazyev, A. J. Austin, R. Cammi, C. Pomelli, J. W. Ochterski, R. L. Martin, K. Morokuma, V. G. Zakrzewski, G. A. S. Voth, P., J. J. Dannenberg, S. Dapprich, A. D. Daniels, Ö. Farkas, J. B. Foresman, J. V. Ortiz, J. Cioslowski and D. J. Fox, *Gaussian, Inc., Wallingford CT*, 2009.
26. X. Y. Cao and M. Dolg, *Journal of Molecular Structure-Theochem*, 2002, **581**, 139-147.
27. X. Y. Cao, M. Dolg and H. Stoll, *Journal of Chemical Physics*, 2003, **118**, 487-496.
28. M. Dolg, H. Stoll, A. Savin and H. Preuss, *Theoretica Chimica Acta*, 1989, **75**, 173-194.
29. B. Ravel and M. Newville, *Journal of Synchrotron Radiation*, 2005, **12**, 537-541.
30. J. J. Rehr and R. C. Albers, *Reviews of Modern Physics*, 2000, **72**, 621-654.

31. G. Ferru, L. Berthon, C. Sorel, O. Diat, P. Bauduin and J. P. Simonin, in *Atalante 2012 International Conference on Nuclear Chemistry for Sustainable Fuel Cycles*, ed. C. Poinssot, Elsevier Science Bv, Amsterdam, 2012, vol. 7, pp. 27-32.
32. S. De Sio, C. Sorel, E. Bosse and P. Moisy, *Radiochimica Acta*, 2013, **101**, 373-377.
33. F. Rodrigues, G. Ferru, L. Berthon, N. Boubals, P. Guilbaud, C. Sorel, O. Diat, P. Bauduin, J. P. Simonin, J. P. Morel, N. Morel-Desrosiers and M. C. Charbonnel, *Molecular Physics*, 2014, **112**, 1362-1374.
34. T. Yaita, H. Narita, S. Suzuki, S. Tachimori, H. Shiwaku and H. Motohashi, *Journal of Alloys and Compounds*, 1998, **271**, 184-188.
35. F. Poineau, M. Fattahi, C. Den Auwer, C. Hennig and B. Grambow, *Radiochimica Acta*, 2006, **94**, 283-289.
36. F. Poineau, P. F. Weck, K. German, A. Maruk, G. Kirakosyan, W. Lukens, D. B. Rego, A. P. Sattelberger and K. R. Czerwinski, *Dalton Transactions*, 2010, **39**, 8616-8619.
37. C. Fillaux, J. C. Berthet, S. D. Conradson, P. Guilbaud, D. Guillaumont, C. Hennig, P. Moisy, J. Roques, E. Simoni, D. K. Shuh, T. Tyliszczak, I. Castro-Rodriguez and C. Den Auwer, *Comptes Rendus Chimie*, 2007, **10**, 859-871.

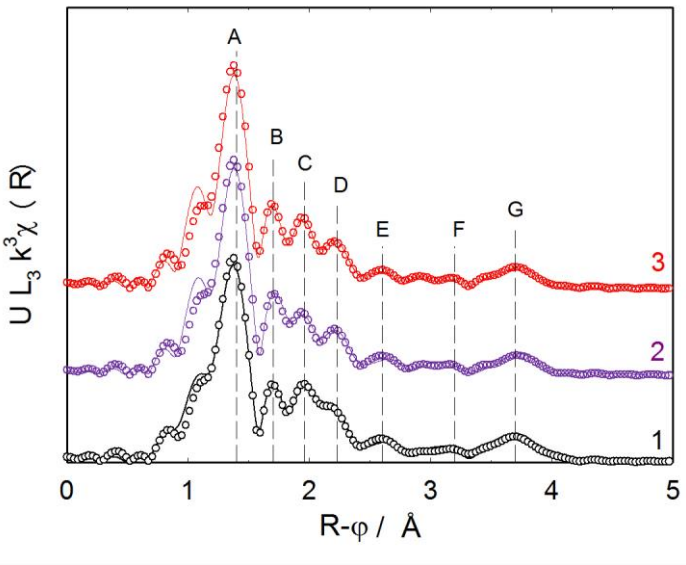


**Figure 5.** Experimental (—) and fitted (◦◦◦) Fourier transform of the $k^3$-weighted EXAFS spectra at uranium $L_3$ edge for organic samples 1 (DEHiBA-uranyl nitrato complexes), 2 and 3 (DEHiBA-uranyl pertechnetate nitrato complexes).

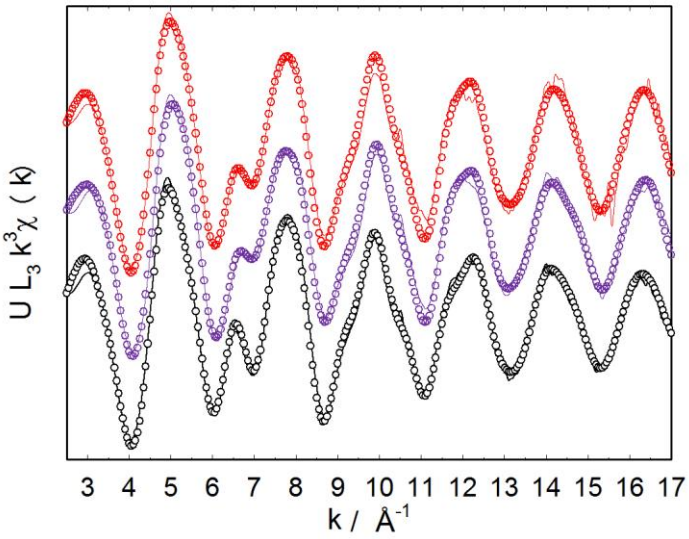


**Figure 6.** Experimental (—) and fitted (◦◦◦) $k^3$-weighted EXAFS spectra at uranium $L_3$ edge for organic samples 1 (DEHiBA-uranyl nitrato complexes), 2 and 3 (DEHiBA-uranyl pertechnetate nitrato complexes).

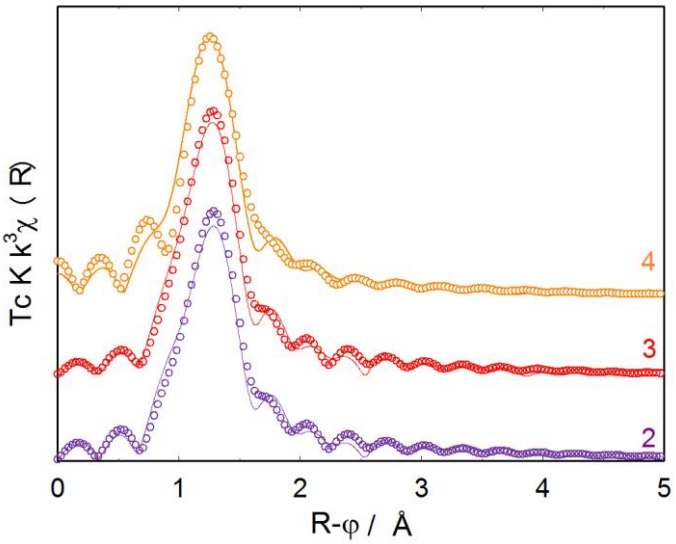


**Figure 7.** Experimental (—) and fitted (◦◦◦) Fourier transform of the $k^3$-weighted EXAFS spectra at technetium K edge for organic samples 2, 3 (DEHiBA-uranyl pertechnetate nitrato complexes) and 4 (DEHiBA- pertechnetate complexes).

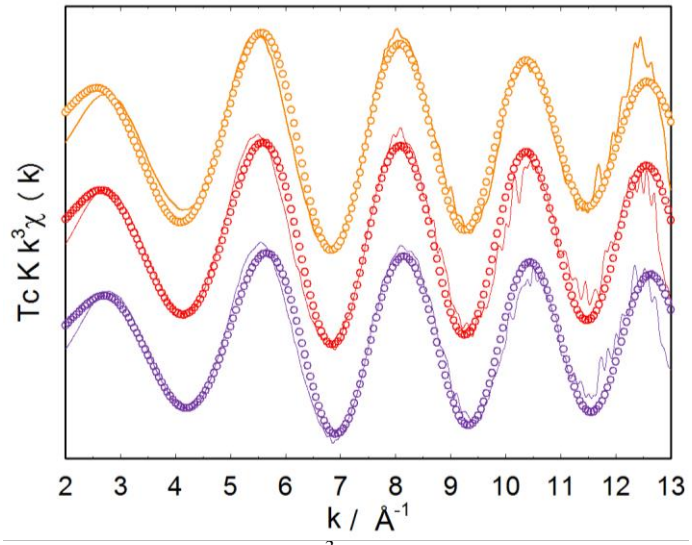


**Figure 8.** Experimental (—) and fitted (◦◦◦) $k^3$-weighted EXAFS spectra at technetium K edge for organic samples 2, 3 (DEHiBA-uranyl pertechnetate nitrato complexes) and 4 (DEHiBA-pertechnetate complexes).